PHYSICAL REVIEW B **78**, 180502(R) (2008)

# Vacuum Rabi splitting due to strong coupling of a flux qubit and a coplanar-waveguide resonator

Abdufarrukh A. Abdumalikov, Jr.,[1,†,*] Oleg Astafiev,[1,2] Yasunobu Nakamura,[1,2,3]
Yuri A. Pashkin,[1,2,†] and JawShen Tsai[1,2,3]
[1]*The Institute of Physical and Chemical Research (RIKEN), Wako, Saitama 351-0198, Japan*
[2]*NEC Nano Electronics Research Laboratories, Tsukuba, Ibaraki 305-8501, Japan*
[3]*CREST-JST, Kawaguchi, Saitama 332-0012, Japan*

(Received 19 August 2008; revised manuscript received 17 September 2008; published 10 November 2008)

We have experimentally studied a superconducting flux qubit strongly coupled to a single mode of a high-quality transmission-type coplanar-waveguide resonator. The qubit-resonator coupling is revealed in the resonator transmission spectrum as a vacuum Rabi splitting. In the dispersive regime the qubit energy levels are spectroscopically probed. We observe a shift in the qubit transition frequency that linearly depends on the number of photons in the resonator, which is attributed to the ac-Zeeman shift. The observations are in agreement with the theoretical predictions.

DOI: 10.1103/PhysRevB.78.180502 PACS number(s): 03.67.Lx

A two-level quantum system (e.g., spin 1/2) coupled to a quantum harmonic oscillator is the object of cavity quantum electrodynamics (cQED). Such systems realized in microwave[1] and optical[2] domains are of great interest in the study of fundamental quantum mechanics of open systems as well as the engineering of quantum states (e.g., squeezed, Schrödinger-cat, and Fock states) and have also been proposed for their use in quantum information processing.[1–3] Ideas for circuit analogs of cQED have recently been proposed and some have been demonstrated using superconducting macroscopic two-level systems (charge,[4–11] flux,[12,13] and phase[14,15] qubits) coupled to electromagnetic or nanomechanical resonators.[16,17] In recent experiments, a quantum state has been stored and coherently transferred between two superconducting phase qubits via a resonator[14] and two charge qubits have been successfully coupled using an on-chip resonator as a quantum bus.[9] Using a charge qubit, single microwave photons have been generated by spontaneous emission[8] and a single artificial-atom maser was experimentally demonstrated.[10] An advantage of superconducting cQED systems over atomic ones is that the qubit energy can be tuned by varying external magnetic field or gate voltage providing control over the qubit-resonator interaction. Moreover, qubits remain at fixed positions and do not suffer from the fact that the coupling energy $g$ varies with position of atoms in the cavity.

Unfortunately, charge qubits in the large charging energy limit suffer from the low-frequency background charge fluctuations. In order to minimize the effect of charge noise which is the main source of decoherence in charge qubits one needs to lower the charging energy by increasing its capacitance with an expense of reduced anharmonicity.[18,19] An alternative approach would be the use of flux qubits instead of charge qubits.[20] Flux qubits are less susceptible to the charge noise while having large anharmonicity. In the previous works on flux qubits, lumped-element resonators with a relatively low-quality factor (Q) have been used[12,13,21] while coupling to high-frequency resonators can be achieved more straightforwardly by using distributed elements such as coplanar-waveguide (CPW) transmission line resonators.[20] With realizable system parameters, a coupling energy $g$ of the order of 100 MHz$\times h$ could be reached while the photon decay rate $\kappa$ from the resonator could be less than $2\pi \times 1$ MHz. Also, recent experiments report the decay rate for flux qubits of the order of $\gamma \approx 2\pi \times 1$ MHz.[22] Thus, the condition for strong coupling $g/h \gg \gamma$; $\kappa$ is readily fulfilled.

In this Rapid Communication, we demonstrate strong coupling between a flux qubit and a microwave field in a high-Q resonator. The transmission spectrum of the system shows vacuum Rabi splitting when the qubit is in resonance with the resonator. In the dispersive regime, the coupling is used to measure level separation between the states of the flux qubit. We also demonstrate that the interaction between the flux qubit and the photon field in the resonator gives rise to a large ac-Zeeman shift of the qubit energy levels depending on the average photon number $\bar{n}$ in the resonator. This effect was observed earlier in atomic systems[23] and with charge qubits.[6]

We use an on-chip superconducting CPW resonator. The resonator is described by the harmonic-oscillator Hamiltonian of $H_r = h\nu_r(a^\dagger a + 1/2)$, where $\nu_r$ is the resonant frequency and $a^\dagger$ and $a$ are the photon creation and annihilation operators, respectively.

The flux qubit is a superconducting loop with four Josephson junctions.[22] Three junctions are designed to be identical while the fourth one is smaller. Under the operating condition of $\Phi \approx \Phi_0/2$, where $\Phi$ is the applied external magnetic flux and $\Phi_0$ is the magnetic-flux quantum, the lowest two energy levels of the qubit are well separated from the higher levels and can be described by the Hamiltonian $H_q = -\frac{1}{2}(\Delta\sigma_x + \varepsilon\sigma_z)$. Here $\Delta$ is the tunneling energy between the two wells of the qubit potential,[24] $\varepsilon = 2I_p(\Phi - \Phi_0/2)$ is the energy bias of the qubit, $I_p$ is its persistent current, and $\sigma_{x,z}$ are Pauli matrices. The qubit parameters such as $I_p$ and $\Delta$ are predetermined during the fabrication process, while the third parameter—the external magnetic flux $\Phi$—is controlled during the experiment.

The qubit is located close to the center of the resonator where the current (and the magnetic field) has an antinode and is coupled to the resonator via the mutual inductance $M$. The corresponding Hamiltonian describing the magnetic-dipole interaction is $H_{\text{int}} = g(a + a^\dagger)\sigma_z$. The coupling constant

 

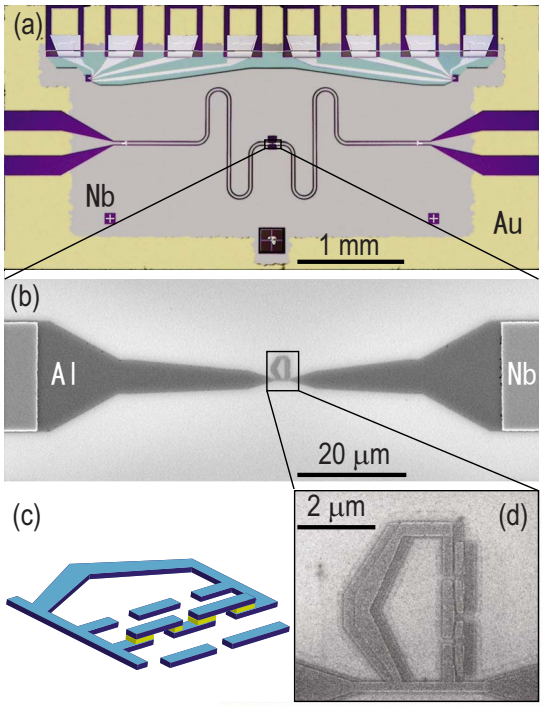


FIG. 1. (Color online) (a) Optical image of the superconducting Nb coplanar-waveguide resonator on a $5\times2.5$ mm$^2$ silicon chip. (b) Electron micrograph of the Al strip with a qubit in the middle overlapping the interrupted Nb central conductor on the left and the right. (c) Schematic view of the qubit. (d) Flux qubit with four Josephson junctions coupled to the resonator via kinetic inductance of the shared part of the Al strip.

is found as $g=MI_pI_{r0}$, where $I_{r0}=\sqrt{h\nu_r/L_r}$ is the zero-point current in the resonator and $L_r$ is the total resonator inductance.

The total Hamiltonian for the coupled system of a harmonic oscillator and a two-level system is, therefore,

$$H=h\nu_r\left(a^\dagger a+\frac{1}{2}\right)-\frac{1}{2}(\Delta\sigma_x+\varepsilon\sigma_z)+g(a+a^\dagger)\sigma_z. \quad (1)$$

The coupling leads to the change in the dressed-state energies of the system from its bare values $h\nu_r(n+1/2)\pm h\nu_a/2$, where $n$ is the photon number in the resonator and $h\nu_a=\sqrt{\varepsilon^2+\Delta^2}$ is the energy-level separation of the bare qubit.

The CPW resonator is fabricated with wet etching of a 200-nm-thick Nb film deposited on a thermally oxidized silicon chip [Fig. 1(a)]. The width of the central conductor is 20 $\mu$m, and the gap between the central conductor and the ground plane is 10 $\mu$m resulting in the wave impedance of about 50 $\Omega$. The resonator is defined by two discontinuities in the central conductor of CPW. The fundamental-mode frequency of the half-wavelength transmission-type CPW resonator is $\nu_r\approx9.907$ GHz. At temperatures $T<50$ mK, much lower than $h\nu_r/k_B\approx500$ mK, the resonator is nearly in its ground state with the thermal photon occupancy $n_{\rm th}<8\times10^{-5}$. The total resonator inductance $L_r\approx2.5$ nH is estimated from its geometry, which gives rise to $I_{r0}\approx52$ nA. The measured quality factor of the resonator is $Q\approx7\times10^3$.

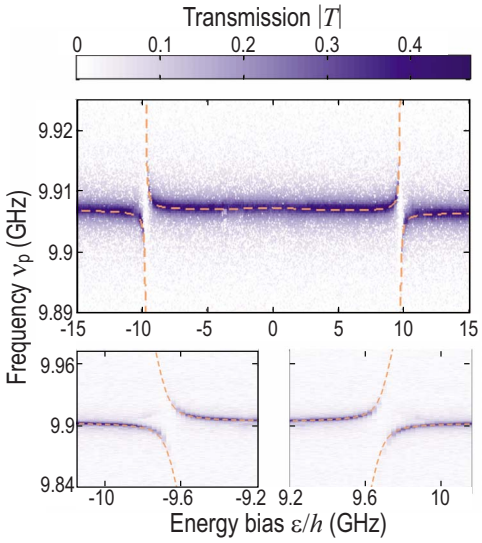


FIG. 2. (Color online) Resonator transmission amplitude $|T|$ plotted versus the probe frequency $\nu_p$ and the qubit energy bias $\varepsilon$. Lower panels are enlarged plots of anticrossings. Dashed lines represent the fitting based on exact solutions of Hamiltonian (1).

The corresponding photon relaxation rate is $\kappa=\nu_r/Q\approx2\pi\times1.4$ MHz.

The central Nb conductor of the resonator is interrupted near its center and an Al strip with a qubit is inserted in the line [Fig. 1(b)]. The Nb-Al interface is formed by a natural Nb oxide. The strip has a constriction and is coupled to the qubit mainly via the kinetic inductance of the shared part. The geometric inductance is negligible in comparison to the kinetic inductance. The strip and the qubit are deposited together using two-angle shadow evaporation technique. The thicknesses of the first and the second Al layers are 20 and 30 nm, respectively. To form the tunnel junctions in the qubit, Al is oxidized in an $Ar+O_2$ mixture before the second layer deposition [Fig. 1(d)].

This qubit-resonator system is characterized by measuring the amplitude $|T|$ and phase $\varphi$ of the microwave transmission coefficient as a function of the probe power $P_p$ and the probe frequency $\nu_p$ using a vector network analyzer. The signal transmitted through the resonator is amplified using a cryogenic amplifier at 4.2 K stage and room-temperature amplifiers. In order to prevent leakage of thermal radiation we use attenuators on the input line and isolators on the output line. The energy bias $\varepsilon$ of the qubit is controlled by the external field applied using a small coil.

The transmission spectrum as a function of the qubit energy bias is shown in Fig. 2. In the measurement we keep the power $P_p$ below $1\times10^{-18}$ W at the input to the resonator, which corresponds to the average number of photons inside the resonator $\bar{n}=P_p/\kappa h\nu_r$ of the order of 0.01 at resonance (see below). This allows us to measure the transitions from the ground state only. By tuning qubit energy $h\nu_a$ to $h\nu_r$, we observe vacuum Rabi splitting, i.e., the anticrossings between the resonator single-photon state and the qubit first-excited state. The anticrossings can be observed when the photon $\kappa$ (i.e., linewidth of the resonator) and the qubit decay rates $\gamma$ are smaller than $g/\hbar$; that is, the strong-coupling

condition is fulfilled. Away from the anticrossings, the qubit and the resonator are effectively decoupled, which is revealed as a resonant transmission at the frequency near $\nu_r$.

In the dispersive limit, when the detuning $\delta=h(\nu_a-\nu_r)$ is large in comparison with $g$, diagonalization of Hamiltonian (1), after transforming into qubit eigenbasis $\sigma_z'$ and using rotating wave approximation, leads to the effective Hamiltonian[4]

$$H \approx \left(h\nu_r - \frac{g_1^2}{\delta}\sigma_z'\right)a^\dagger a - \frac{1}{2}\left(h\nu_a + \frac{g_1^2}{\delta}\right)\sigma_z', \qquad (2)$$

where $g_1=g\sin\theta$ and $\theta=\arctan(\Delta/\varepsilon)$. The first term describes the dependence of the resonator frequency on the qubit state $\sigma_z'$, the detuning $\delta$, and the coupling energy $g$. Thus, the state of the qubit can be inferred from the measurement of the resonator frequency. On the other hand, the level separation of the qubit $h\tilde{\nu}_a=h\nu_a+2ng_1^2/\delta+g_1^2/\delta$ depends on the number of photons in the resonator. The second term proportional to $n$ corresponds to the ac-Zeeman effect, and the last term corresponds to the Lamb shift.

In order to find the level separation of the qubit, we measure the phase $\varphi$ of the transmitted probe signal depending on the qubit states.[6] The probe frequency is adjusted to maximum transmission through the resonator, which takes place at $\nu_p=\nu_r-g_1^2/h\delta$ when the qubit is in the ground state. The qubit is then excited by applying an additional continuous-wave (cw) microwave of frequency $\nu_e$ through the same input port as the probe signal. For a large amplitude drive, the populations of the qubit ground and excited states approach 1/2 when $\nu_e$ matches $\tilde{\nu}_a$. In this case, the change in phase $\varphi$ is expected to saturate at $\delta\varphi=\arctan(g_1^2/\hbar\delta\kappa)$. By sweeping $\nu_e$ and $\varepsilon$, we have mapped out the qubit energy-level separation $h\tilde{\nu}_a$ [Fig. 3(a)]. The phase shift due to the qubit excitation is observed as narrow dark (below 9.9 GHz) and bright (above 9.9 GHz) lines. As expected, for $h\nu_a<h\nu_r$ we observe a negative change; while at $h\nu_a>h\nu_r$ the phase change is positive and decreases with the qubit energy. Note that we can distinguish the qubit states even at its degeneracy point $\varepsilon=0$. Using this technique, we have also measured the spectrum of the higher levels of the qubit (not presented in this Rapid Communication).

The spectroscopy results are fitted to the eigenstate of the full Hamiltonian of the four-junction flux qubit [Fig. 3(b)]. From the fitting, we find the charging energy of the large junctions $E_C\approx 2.67$ GHz$\times h$, their Josephson energy $E_J\approx 153$ GHz$\times h$, and the ratio of the small and the large junctions $\alpha\approx 0.58$. The persistent current is found from the external flux positions of two anticrossings to be $I_p\approx 144$ nA. Using these parameters we fit the observed vacuum Rabi splitting by diagonalizing Hamiltonian (1) (dashed lines in Fig. 2) (Ref. 25) and obtain the coupling energy $g\approx 120$ MHz$\times h$. This gives an estimate of the mutual inductance $M=g/I_pI_{r0}\approx 10.7$ pH, which is close to the designed value of 15 pH.[26]

For the spectroscopy we have used the dependence of the resonator frequency on the state of the qubit. Correspondingly, the resonator acts back onto the qubit through their mutual coupling. In order to characterize the effect of this

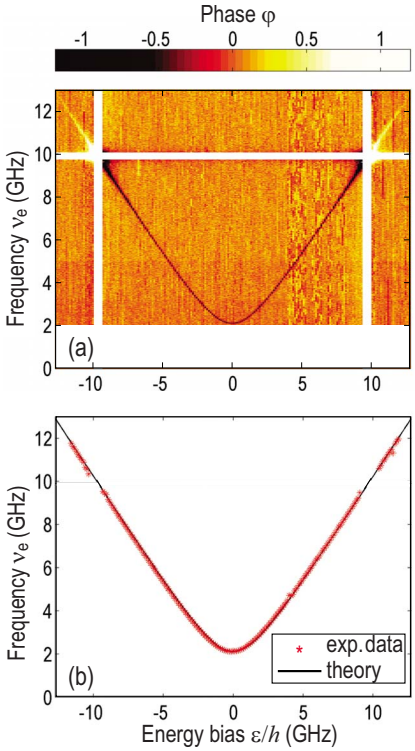


FIG. 3. (Color online) (a) Intensity plot of phase $\varphi$ as a function of energy bias $\varepsilon$ and exciting frequency $\nu_e$. White stripes correspond to the regions not measured. (b) Comparison of the experimentally found level separation (symbols) with the fitting based on exact solutions of the full Hamiltonian (line).

"back action," we measure the qubit spectrum at $\varepsilon=0$ for various probe power $P_p$. In the low power limit $P_p\to 0$, the qubit has a level separation $h\tilde{\nu}_a=h\nu_a+g_1^2/\delta\approx 2.12$ GHz$\times h$ though the small Lamb shift is not resolved experimentally. With increasing $P_p$, $h\tilde{\nu}_a$ shifts linearly (Fig. 4), which is attributed to the ac-Zeeman shift. At this particular energy bias $\varepsilon=0$, the ac-Zeeman shift due to one photon is calculated to be $2g^2/\delta\approx -3.8$ MHz$\times h$. Thus, the dependence of the average intraresonator photon number $\bar{n}$ on the input power $P_p$ can now be determined. With this relation, the probe power level used in the measurements of the vacuum Rabi splitting and the qubit spectrum is calibrated to be $\bar{n}\approx 0.01$.

In our experiments, we have achieved a strong coupling of a superconducting transmission-type resonator with a flux

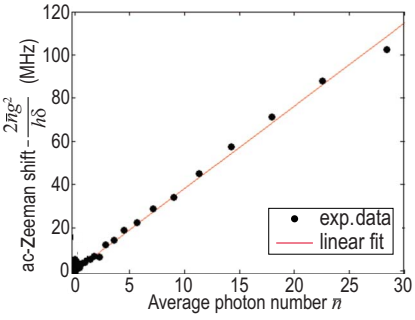


FIG. 4. (Color online) Comparison of the experimentally found level separation shift (symbols) with a linear fit (line).

qubit, which is demonstrated by the observation of the vacuum Rabi splitting in the transmission spectrum of the resonator. In the dispersive regime, the strong coupling leads to the shift of the resonator frequency depending on the qubit states. Using this property we measured spectrum of the qubit. We also observed the ac-Zeeman shift of the qubit level separation due to the photon field in the resonator. The agreement with theoretical predictions demonstrates that a flux qubit coupled to a resonator is a well-tailored system for cavity-QED experiments.

We would like to thank Kunihiro Inomata and Tsuyoshi Yamamoto for their help to set up the measurement system and Alexandre Blais for helpful discussions.

*abdumalikov@frl.cl.nec.co.jp. On leave from Physical-Technical Institute of the Academy of Sciences, Uzbekistan.

†On leave from Lebedev Physical Institute, Moscow 119991, Russia.

[1] J. M. Raimond, M. Brune, and S. Haroche, Rev. Mod. Phys. **73**, 565 (2001).

[2] H. Mabuchi and A. C. Doherty, Science **298**, 1372 (2002).

[3] C. J. Hood, T. W. Lynn, A. C. Doherty, A. S. Parkins, and H. J. Kimble, Science **287**, 1447 (2000).

[4] A. Blais, R.-S. Huang, A. Wallraff, S. M. Girvin, and R. J. Schoelkopf, Phys. Rev. A **69**, 062320 (2004).

[5] A. Wallraff, D. I. Schuster, A. Blais, L. Frunzio, R.-S. Huang, J. Majer, S. Kumar, S. M. Girvin, and R. J. Schoelkopf, Nature (London) **431**, 162 (2004).

[6] D. I. Schuster, A. Wallraff, A. Blais, L. Frunzio, R.-S. Huang, J. Majer, S. M. Girvin, and R. J. Schoelkopf, Phys. Rev. Lett. **94**, 123602 (2005).

[7] D. I. Schuster, A. A. Houck, J. A. Schreier, A. Wallraff, J. M. Gambetta, A. Blais, L. Frunzio, J. Majer, B. Johnson, M. H. Devoret, S. M. Girvin, and R. J. Schoelkopf, Nature (London) **445**, 515 (2007).

[8] A. A. Houck, D. I. Schuster, J. M. Gambetta, J. A. Schreier, B. R. Johnson, J. M. Chow, L. Frunzio, J. Majer, M. H. Devoret, S. M. Girvin, and R. J. Schoelkopf, Nature (London) **449**, 328 (2007).

[9] J. Majer, J. M. Chow, J. M. Gambetta, J. Koch, B. R. Johnson, J. A. Schreier, L. Frunzio, D. I. Schuster, A. A. Houck, A. Wallraff, A. Blais, M. H. Devoret, S. M. Girvin, and R. J. Schoelkopf, Nature (London) **449**, 443 (2007).

[10] O. Astafiev, K. Inomata, A. O. Niskanen, T. Yamamoto, Yu. A. Pashkin, Y. Nakamura, and J. S. Tsai, Nature (London) **449**, 588 (2007).

[11] J. M. Fink, M. Göppl, M. Baur, R. Bianchetti, P. J. Leek, A. Blais, and A. Wallraff, Nature (London) **454**, 315 (2008).

[12] I. Chiorescu, P. Bertet, K. Semba, Y. Nakamura, C. J. P. M. Harmans, and J. E. Mooij, Nature (London) **431**, 159 (2004).

[13] J. Johansson, S. Saito, T. Meno, H. Nakano, M. Ueda, K. Semba, and H. Takayanagi, Phys. Rev. Lett. **96**, 127006 (2006).

[14] M. A. Sillanpää, J. I. Park, and R. W. Simmonds, Nature (London) **449**, 438 (2007).

[15] M. Hofheinz, E. M. Weig, M. Ansmann, R. C. Bialczak, E. Lucero, M. Neeley, A. D. O'Connell, H. Wang, J. M. Martinis, and A. N. Cleland, Nature (London) **454**, 310 (2008).

[16] A. D. Armour, M. P. Blencowe, and K. C. Schwab, Phys. Rev. Lett. **88**, 148301 (2002).

[17] E. K. Irish and K. C. Schwab, Phys. Rev. B **68**, 155311 (2003).

[18] J. Koch, T. M. Yu, J. Gambetta, A. A. Houck, D. I. Schuster, J. Majer, A. Blais, M. H. Devoret, S. M. Girvin, and R. J. Schoelkopf, Phys. Rev. A **76**, 042319 (2007).

[19] J. Q. You, X. Hu, S. Ashhab, and F. Nori, Phys. Rev. B **75**, 140515(R) (2007).

[20] T. Lindström, C. H. Webster, J. E. Healey, M. S. Colclough, C. M. Muirhead, and A. Y. Tzalenchuk, Supercond. Sci. Technol. **20**, 814 (2007).

[21] E. Il'ichev, N. Oukhanski, A. Izmalkov, T. Wagner, M. Grajcar, H.-G. Meyer, A. Y. Smirnov, A. M. van den Brink, M. H. S. Amin, and A. M. Zagoskin, Phys. Rev. Lett. **91**, 097906 (2003).

[22] F. Yoshihara, K. Harrabi, A. O. Niskanen, Y. Nakamura, and J. S. Tsai, Phys. Rev. Lett. **97**, 167001 (2006).

[23] M. Brune, P. Nussenzveig, F. Schmidt-Kaler, F. Bernardot, A. Maali, J. M. Raimond, and S. Haroche, Phys. Rev. Lett. **72**, 3339 (1994).

[24] For the parameters of the flux qubit investigated in this paper, the barrier between the potential minima is lower than the ground-state energy level. Nevertheless, the qubit Hamiltonian is valid for describing our flux qubit.

[25] The small magnetic-field dependence of the resonator frequency ($\sim$0.5 MHz across Fig. 2) is taken into account with a linear interpolation.

[26] A. O. Niskanen, K. Harrabi, F. Yoshihara, Y. Nakamura, and J. S. Tsai, Phys. Rev. B **74**, 220503(R) (2006).